SLAC-PUB-9497
September 2002

Neural Network Analysis of LEAP Energy Spectra.

Robert Holdridge

Energy Research Undergraduate Laboratory Fellowship

Cabrillo College

Stanford Linear Accelerator Center, Stanford, CA 94309

September 6 2002

Prepared in partial fulfillment of the requirements of the Office of Science, Department of Energy-Energy Research Undergraduate Laboratory Fellowship under the direction of Helen Quinn at the Stanford Linear Accelerator Center.

Participant: _____
Signature

Research Advisor: _____
Signature

Work supported in part by the Department of Energy contract DE-AC03-76SF00515.

Abstract

Neural Network Analysis of LEAP Energy Spectra.
Robert Holdridge (Cabrillo College, Aptos, Ca. 95003)

The Laser Electron Acceleration Project (LEAP) group has been conducting a proof of principle experiment on the acceleration of electrons with a pair of crossed laser beams. To date there has been no experimental verification of electron acceleration with crossed laser beams in a dielectric loaded vacuum, although the energy profile of an accelerated electron bunch has been well described by theory. The experiment is subject to unavoidable time dependent fluctuations in the independent variables. Changes in the experimental parameters can dramatically alter the beam profile incident near the focal plane of a high-resolution spectrometer located downstream from the accelerator cell. Neural networks (NNs) appear to provide an ideal tool for the positive determination of an acceleration event, being adaptable and able to handle highly complex nonlinear problems. Typical NNs under such conditions require a training set consisting of a representative data set along with "answers" which have been determined to be consistent with the variable state of the experimental parameters. A strategy of pattern recognition with respect to the status of independent variables can be employed to determine the signature characteristics of a laser perturbed electron bunch. Data cuts representing characteristics that were thought to be distinctive to accelerated beam profile images were implemented in the algorithm employed. Statistical analysis of the results of data cuts made on the energy profile images from the experiment is presented, as well as conclusions drawn from the results of this analysis. Finally, a discussion of future directions to be taken in this work is given including the orientation towards on-line, real-time analysis.

Introduction

The goal of the LEAP program is to perform an experiment that clearly demonstrates laser acceleration in a dielectric loaded vacuum. Among the practical advantages of the acceleration of an electron bunch under these conditions are higher energy gradients than conventional RF linear accelerators and the absence of material that could deteriorate the electron beam quality, as in plasma based laser accelerators. The damage threshold of the accelerator structure from the electric field is the limiting factor for the acceleration gradient. Structures constructed from dielectric materials are capable of withstanding higher electric fields before losing structural integrity than structures made from conductive materials. The increase in achievable gradient is approximately an order of magnitude above that of conventional RF accelerators.[i]

Data collected from the experiment consists of energy spectrometer images produced by the interaction of the electron beam with the YAG screen near the focal plane of a high resolution spectrometer. Following acceleration by the laser, the images should show a symmetric widening of the electron beam profile, as expected by theory.[ii]

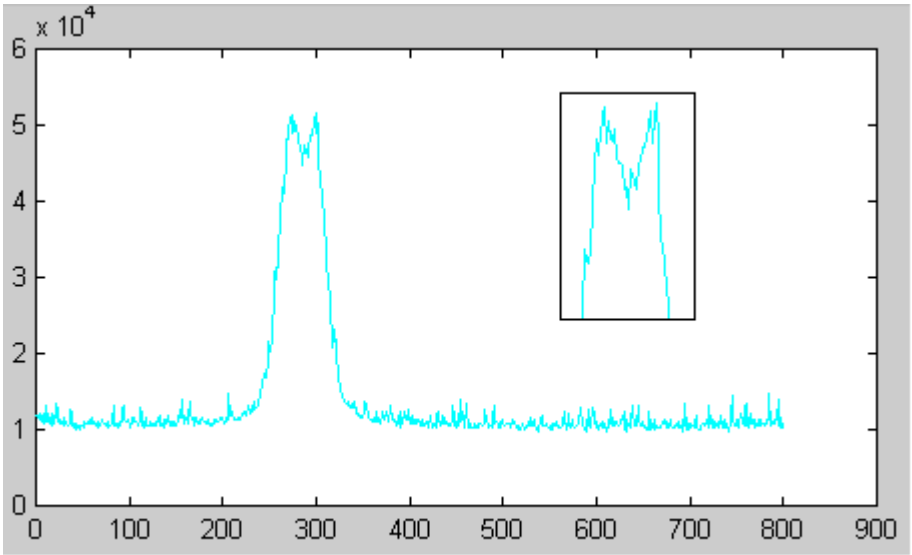

Fig 1: An energy specrtometer image of e-beam profile

The bifurcated peak, as shown in the inset of Fig. 1, is recognized as a signature of an accelerated beam whose degree depends on the acceleration gradient for unbunched electrons because the acceleration of a portion of the electron bunch will be accompanied by an equivalent deceleration of another portion of the electron bunch.[iii] While an analytic numerical description of such a nonlinear shape is possible, a neural network (NN) implementing a pattern recognition strategy is desirable in order to identify the positive acceleration events in post experimental data analysis as well as during online, real-time data acquisition. NNs, which can learn and modify rules as the knowledge domain changes, have been shown to be effective at adaptive learning in unknown, incomplete or noisy environments.[iv]

To provide a training set for the NN, the data sets will be divided into events that will provide a logical classification of the data. For example, the state of laser toggling (On / Off) will be noted so as to give the NN a baseline to work from. Correctly parsed data will allow for the determination of distinctive characteristics, such as the bifurcated peak shown in the inset of Fig. 1 that would indicate an observable acceleration gradient through the accelerator cell. Among the changes expected in an accelerated beam profile image are a bifurcation of the energy distribution near the peak and an increase in the beam profile width on the cleaner, high-energy or “back porch” side of the beam profile.

The use of NNs to analyze by way of pattern recognition the data from the LEAP experiment should allow for the positive determination of the viability of laser acceleration of an electron beam. As a result of the inherent speed obtained by parallel computational architectures, recognized by combinatorial rather than sequential data processing, it could be possible for real time decisions regarding data acquisition and system status control to be made by employing NNs for data analysis or acquisition.

Materials and Methods

The programming work on this research project was performed on the Windows NT platform installed on a Dell Optiplex machine with an x86 Pentium chip. The primary application employed in the programming was MatLab version 5.3 from Math Works. The programming code used by MatLab is similar to the C language with additional application specific features including matrix manipulation and extensive graphing capabilities. Microsoft Excel was also used to facilitate numerical and graphical analysis of the data sets.

The data sets analyzed were taken from data gathered during the June 2002 run of the LEAP experiment. Data consisted of a three dimensional matrix representing the sequential images of the energy density of electron beam profile images collected by an image intensified CCD camera looking at the focal plane of a high resolution spectrometer. The camera has dimensions of 512 pixels high by 1024 pixels wide, with the larger dimension corresponding to the dispersion direction of the spectrometer. The number of images in an experimental run determines the third dimension of the data set matrix. Data was entered into the image matrices using software from National Instruments. In order to obtain reduction of data set size and backwards compatibility with previously collected data, the columnar energy values obtained were summed and binned resulting in a vector pixel array representing the energy density of the electron beam across the focal plane of the spectrometer. Calibrating the pixel array against the known screen size of the CCD and dispersion of the spectrometer gives the keV / pixel, or the energy distribution. The calibration of the pixel array led to a value of 0.92 keV / pixel.

In addition to beam profile images, the data also contained an additional array containing the parameters of the particular experimental run. Of primary importance in this array were values indicating the Laser ON / Laser OFF (L1 / L0) status and the time step, which gives the

timing separation between the laser pulse and the occurrence of an electron bunch in the accelerator cell in picoseconds. Timing differences between the variable length laser pulse and the occurrence of an electron bunch in the accelerator cell were made pseudo-random in order to prevent bias. The time step, in picoseconds, is important in helping to identify the laser-electron acceleration events and the optimum timing between the electron bunch and laser pulse in order to produce acceleration of the beam. All potential acceleration events should be clustered in time within a few picoseconds to be considered valid.

In analyzing the data, the prime feature of importance in a beam profile was the magnitude (MPI) and location (XPI) of peak intensity in each image. This value was obtained by the built in max (X) function in MatLab which returns the largest value in matrix X and its columnar pixel location. The identification of the XPI was considered to be of primary importance in analyzing the images as it provided a relative offset factor when considering the shape of individual beam profiles. The MPI and XPI values were added to a matrix, *PIvalues*, along with the L1 / L0 status bit.

After obtaining the MPI and XPI, one could obtain approximations to the profile relative to these values for comparison of images. The program searched for horizontal pixel locations representing the desired intensity values from 10% to 90% of the MPI. The algorithm was constructed in such a way so as locate the pixel nearest to the desired percentage intensity. Although linear interpolation of the data would have provided a greater degree of precision in the location of percentage intensity, integer values were chosen over floating point numbers in assigning a horizontal pixel location of percentage intensity for the reasons of speed and simplicity. The use of integers also allowed for a distinct pixel value to be assigned to each percentage location. Percentage values of the MPI were searched inward, from the edges of the

image towards the XPI, and outward, from the XPI to the edges of the image. The primary division in the graphical interpretation of the beam image is the peak intensity. The high-energy side of the profile is here referred to as the "back porch", while the low energy side of the profile is referred to as the "front porch". The percentage intensity pixel values were added to the *PIvalues* matrix in four separate groupings, front and back porches searching outward from the XPI towards the edges, and front and back porches searching inward from the edges towards the XPI.

Having the XPI and percentage intensity locations, the algorithm then calculated the widths from the XPI to each of the pixels representing the percentage intensity locations for each run. These values are referred to as the profile data array and were added to the *PIvalues* matrix in four separate cell groupings, a "front porch" and "back porch" data array, searched outwards and inwards.

In the sequential processing of images in the data set, the next step was to calculate the mean values and root mean squared values of the XPI locations and the percentage intensity locations. The mean profile widths from 10% to 90% of the MPI and the associated root mean squared values for the experimental run of images were also calculated. The results of these calculations were binned into two groups, L1 and L0 determined from information obtained from the original data sets, and were added to the vectors L0meanWidth and L1meanWidth.

At this point in the program, the algorithm has constructed a matrix, *PIvalues*, which indicates, for each image, the L1 / L0 status, MPI, XPI, percentage intensity locations of 10%-90% of MPI for both the front and the back porches searched from the edges to the XPI and from the XPI to the edges, and the beam profile widths at percentage intensities from 10%-90%. The algorithm has also calculated the mean XPI, the mean percentage intensity locations from 10%-

90%, the mean beam profile widths from 10%-90% and binned the results in either L1 or L0 vectors. The algorithm has also determined the root mean square values associated with the above calculations.

After constructing the above matrix, the algorithm proceeds to bin the images according to a strategy outlined by the possible changes in the beam profile as expected by theory.

Data Cuts

The first data cut to be made in order to logically bin the images was a search for asymmetry about the XPI in the upper portions of the beam profile in the 80%-90% range. By comparing the "back porch" edge to peak profile with the "back porch" peak to edge profile, images that contain conflicting values relating to beam width are flagged with a logical yes in cell number 76 (F. 76) of the *PIvalues* matrix. Disagreement between the two profiles indicates the location of local maxima in the beam profile. (Fig. 2) The results of this data cut are binned into L1 and L0 images.

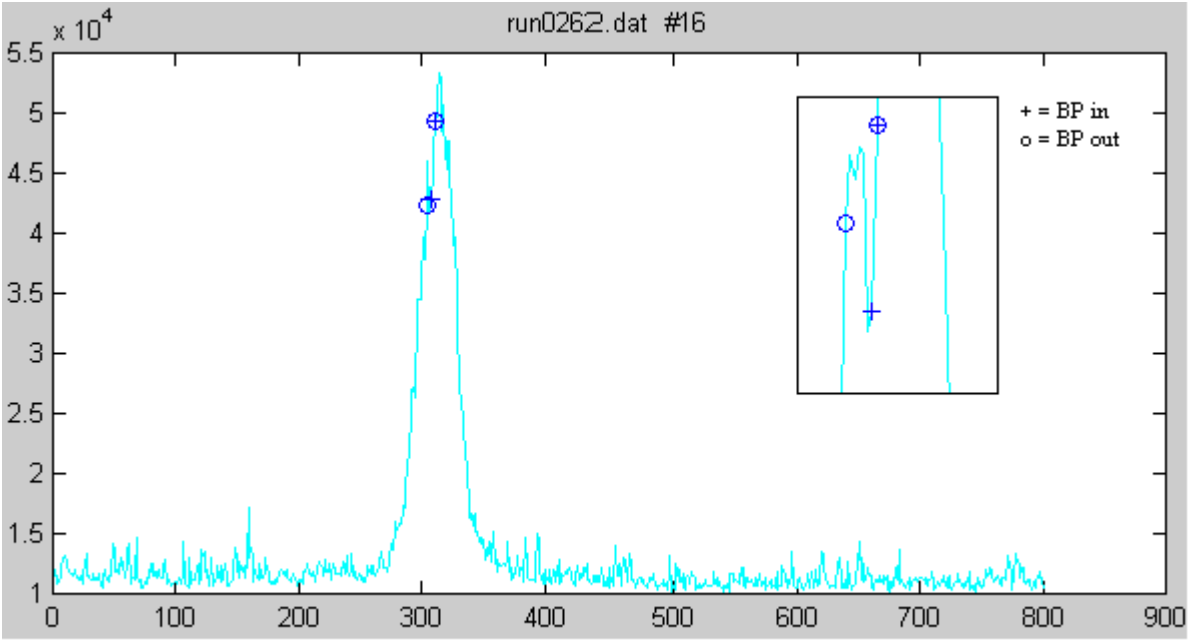

Fig 2: Electron beam profile with 80% and 90% MPI indicated by symbols. Inset: Close-up of back porch region where profile widths do not coincide, resulting in flagging the image for asymmetry.

The second cut that was made on the data was related to the XPI, the L1 / L0 bit and the mean L1 XPI. In accordance with theory, which indicates that an acceleration event will result in the increase of energy spread of that electron bunch, the XPIs of L1 flagged images were compared to the mean XPI of all L1 images in the data set. Images that had an XPI indicating a higher energy than the mean L1 XPI of that run set F. 77.

The above data cuts were combined to determine the correlation of asymmetrical beam profiles to XPI location. An image would set F. 79 if it showed asymmetry in the 80% to 90% range and if its XPI was located in a higher energy region than the mean XPI for all L1 images in the run being analyzed.

An additional binning of the images from an experimental run resulted in a group of benchmark images. Benchmark images were classified as being L0 and symmetrical about the XPI in the 70% to 90% region of the beam profile. These images are used as a benchmark of an electron beam profile without the effects of laser interaction.

As a result of the anticipated widening of the beam profile due to acceleration of the electron bunch by the pair of crossed laser beams, conditional algorithms were established to analyze the relation of profile widths to a variety of metrics calculated for each data set. F. 78 was set when the image showed a widening of the 20% to 40% region of the beam profile when compared to benchmark images.

A further use of profile widths calculated from L0 flagged images was in setting F. 80: the comparison of the 70% to 90% “back porch” profile widths of L1 flagged images with the root mean squared values associated with the distribution of L0 percentage profile widths in the same region of the beam profile. It was anticipated that acceleration events would produce summed

profile values that were greater than the summed values of the L0 images.

Additionally, F. 81 was set when any L1 image had a greater summed profile value than the sum of mean L0 profiles in the upper half (50%-90%) of the beam profile. It was thought that a widening of the 50% to 90% region of the "back porch" profile of L1 flagged images that showed signs of acceleration would be apparent when compared to a benchmark type image.

Another Boolean conditional algorithm employed in the analysis of the data sets was based on the unfounded idea that a positive acceleration gain would be more distinguishable in the higher energy "back porch" than on the "front porch". This algorithm compared the profile sums in the 70% to 90% portion of the back and front porches, setting F. 82 and displaying the results in L1 and L0 bins.

The final data cut employed in the identification strategy employed is related to the decrease in the peak energy intensity associated with energy profile widening resulting from acceleration by the crossed laser beams. F. 83 was set when the image MPI was less than the L0 mean MPI.

F. 78, F. 79, F. 80, F. 81, F. 82 and F. 83 were logically ANDed together at the end of the data analysis program. Images in the data set that satisfied all of the above stated conditions set F. 84 and their image numbers were displayed on the monitor for reference while viewing selected images of the experimental run. A time step was then added to the *PIvalues* matrix to indicate at what point in the 100 picosecond time scan envelope the image was acquired.

Results

Using the output determined by the 6 conditional low-level algorithms, the images were binned according to their L1 / L0 bit. In each case a percentage was calculated from the L1 / L0 status of the flagged image divided by the total number of L1 / L0 images in the particular run.

A detailed analysis of the results obtained from the above-calculated percentages on a semi-continuous group of thirteen experimental runs was conducted. It was found that the mean ratio of percentage of flagged L1 images possible to the percentage of L0 flagged images possible was unity with a σ value of 0.032. This indicates that each flag that was set produced the effect of cutting the number of images in the L1 and L0 bins by nearly equal percentages. It was anticipated that the identified characteristics would result in a higher percentage of L1 images being flagged than L0 images.

Selecting a data set at a random from the experimental runs considered in the analysis above, the effects of the flags can be seen. According to the strategy adopted, each data cut as represented by the flagging algorithms should have the effect of winnowing the pool of images which may represent events of positive acceleration of the electron beam. Tabular results which represent the effect of data cuts employed in the identification strategy are presented in Table 1.

Data from Run0279 taken on June 26, 2002 consists of 3002 images. The data was binned into 2412 L1 images (80.3%) and 590 L0 images (19.7%), a ratio of four to one which was consistent through the last 20 data sets obtained in the June 2002 experimental run.

The test for asymmetry about the peak, F. 76, resulted in 354 L1 images being flagged, 14.7% of all L1 images. 13.9% of all L0 images were also flagged by this test. While this is a considerable reduction in the pool of images representing acceleration events, the nearly equal percentage of L0 events eliminated was nearly equal to L1 events. (L1:L0 = 1.09)

Table 1 Tabulated results from flagging algorithms on run0279

3002 Images	**2412 L1**	**590 L0**	**Run0279**	**26-Jun-02**		
Flag 76: Two Peaks			436 Flagged Images			
			354 L1	15% of L1		
			82 L0	14% of L0	Images remaining in set:	354
Flag 77: XPI<meanL0 XPI			1742 Flagged Images			
			1387 L1	58% of L1		
			355 L0	60% of L0	Images remaining in set:	223
Flag 78: Wider at 20-40% than L0 mean width			653 Flagged Images			
			533 L1	22% of L1		
			120 L0	20% of L0	Images remaining in set:	93
Flag 80: Wider at 70-90% than L0 mean width			1435 Flagged Images			
			1160 L1	39% of L1		
			275 L0	47% of L0	Images remaining in set:	53
Flag 81: Wider at 50-90% than L0 mean width			1573 Flagged Images			
			929 L1	39% of L1		
			229 L0	39% of L0	Images remaining in set:	44
Flag 82: Back Porch > Front Porch at 70-90%			1432 Flagged Images			
			1147 L1	48% of L1		
			285 L0	48% of L0	Images remaining in set:	36
Flag 83: MPI < meanL0 MPI			1782 Flagged Images			
			1424 L1	59% of L1		
			358 L0	61% of L0	Images remaining in set:	36

F. 77, which tested for an XPI location of higher energy than the mean L1 XPI location,

flagged a total of 1743 images, 1387 L1 and 355 L0 (56% of L1 and 60% of L0). This flag left 223 L1 images remaining that might represent a positive acceleration gradient.

F. 78 tested all L1 images for wider beam profile than the L0 mean width in the 20% to 40% MPI range. This data cut resulted in 533 flagged images (22% of L1 images). L0 images were also checked and it was found that 120 L0 images were flagged (20% of L0 images). F. 78 left 93 images remaining as possible 'events'.

F. 80, which represented a wider beam profile in the 70% to 90% MPI range of the "back porch" of L1 images than the rms value of all L0 images, resulted in 1160 L1 images being flagged (39% of L1 images). This data cut was also checked for L0 images, of which 275 were flagged (47% of L0 images). This test reduced the set of possible L1 positive acceleration images to 53.

F. 81 represented a wider beam profile of all images in the 50% to 90% MPI range, when compared to the L0 mean profile widths in the 50% to 90% MPI range. This test resulted in 1573 images being flagged. 929 L1 images (39%) were flagged and 229 L0 images (47%) were flagged. From the available pool of 53 L1 images, 44 images were flagged.

F. 82 was set when the summed 70% to 90% MPI profile widths were identified as being greater on the "back porch" than the equivalent sum of profile widths on the "front porch" when the percentage MPI locations were searched from the edges towards the XPI. This test resulted in 1432 images being flagged, 1147 L1 images (47.6%) and 285 L0 images (48.3%), leaving 36 L1 images that could represent positive acceleration according to the strategy that was adopted.

F. 83 was set when the MPI of the image was less than the mean MPI of all L0 images. This data cut resulted in 1424 of all L1 images (59%) being flagged and 358 of all L0 images

(61%) being flagged. Due to the sequential arrangement of flagging algorithms, this data cut did not result in winnowing of the pool of possible acceleration events, leaving a total of 36 L1 images as potential acceleration events.

Conclusions and Discussion

Statistical analysis of the beam profiles has yet to provide a definitive answer as to whether positive acceleration events have occurred. Barring insufficiently comprehensive data sets or lack of knowledge of the status of variable parameters of the experimental equipment, all logically sound algorithms geared towards problem solving should arrive at the same conclusions. This is related to reproducibility at the foundation of all scientific research. In this sense my research has been a success in reproducing the results from earlier attempts at the analysis of the acquired data.

The bifurcated peak was initially thought to be a signature characteristic of the image of an electron bunch affected by laser acceleration. Following the visual analysis of hundreds of images, both L0 and L1, it can be safely stated that the presence of a bifurcated peak is not necessarily concomitant to an acceleration event due to variations in laser regen power.

Undocumented variance of experimental parameters i.e. accelerator cell slit width, energy of the crossed laser beams in the accelerator cell, the mode of the laser's operation, damage to the accelerator cell and confusion concerning the status or stability of the independent variables as recorded in the LEAP logbook also caused a hurdle in the determination of a set of conditions necessary for laser acceleration of electrons.

In the final step of the data analysis, the strategy employed failed to find a definite correlation between the time step of the image and peaks flagged for possible acceleration. Fig.3 represents a histogram of the total number of images (3002) occurring in one picosecond bins

throughout the time separation of 210 to 310 picoseconds during this run. As can be seen from the figure, the images are well distributed throughout the scan range.

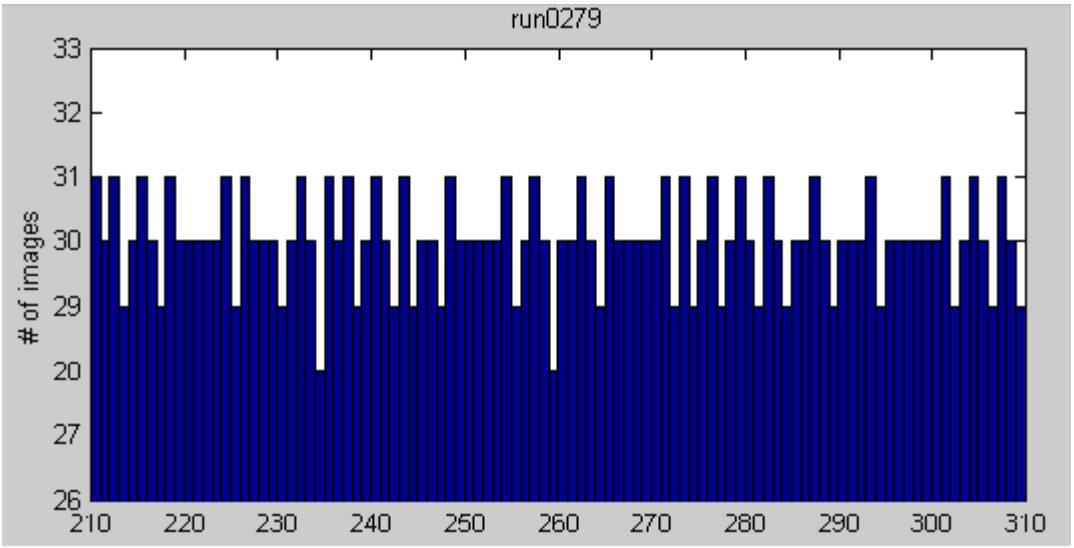

Fig. 3 Histogram representing number of images across a scan range of 210 to 310 picoseconds

The results from the event identification strategy can be seen in Figs. 4 and 5. In Fig. 4, the images that were flagged as possible acceleration events are binned into five picosecond bins and represented in a histogram identifying the number of events associated with the bin of the indicated time step. The mean of this distribution is 1.8 events and the related σ value is 1.24. One, two and three σ values are indicated on the histogram. In the future, peaks such as the one observable at ~255 picoseconds which is statistically significant can be correlated with the regen power of the laser to determine any apparent connection between laser power, the appearance of a peak or not in any run, as well as the degree of bifurcation of the energy profile.

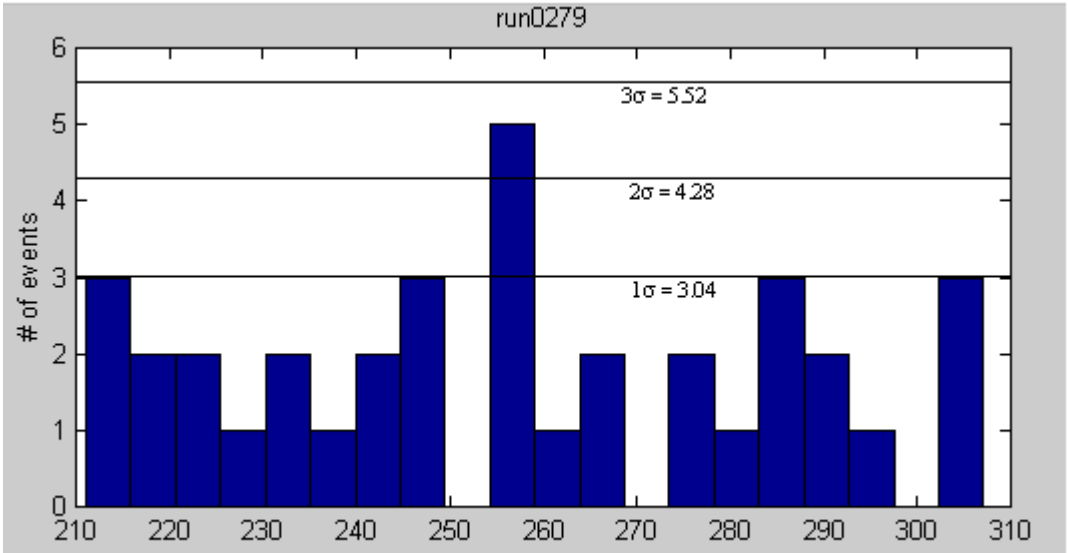

Fig. 4 Histogram of events over scan range in five picosecond bins

Fig. 5 shows the histogram identifying the flagged events with the scan range separated into one picosecond bins. The mean of this distribution is 0.72 events with an associated σ value of 0.61. Again, one two and three σ values are shown on the histogram.

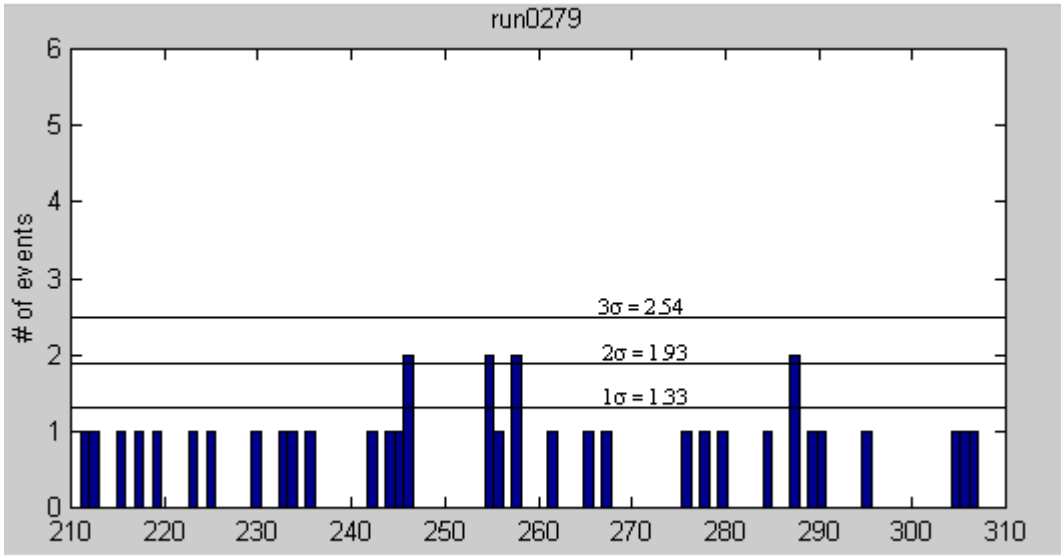

Fig. 5 Histogram of events over scan range in one picosecond bins

What initially appeared in Fig. 4 to be promising results from the identification strategy using five picosecond bins for the scan range became ambiguous, due to lack of statistics, when the scan range was binned in one picosecond bins. As evidenced by Fig. 5, the change of time

binning can result in the appearance, or disappearance of statistically significant events because of the lack of sufficient events. Given consistency in the correct acquisition of time separation between the electron bunch and laser pulse, multiple runs could be combined to improve the statistics necessary for clear observation of laser acceleration of electrons.

Further work with neural networks applied to this problem should combine the available data in such a way so as to make possible more detailed statistical analysis of the results. Additionally, images that are identified as being representative of acceleration events could be analyzed more thoroughly in order to determine particular characteristics of the beam profiles of these images. Furthermore, analysis on the interrelation of data cuts can be made in order to determine the correlation of characteristics flagged by the algorithms. For example, F. 83 flagged 59% of L1 images but failed to winnow the remaining set of images, indicating a correlation between a decrease in the maximum peak intensity and at least one other characteristic employed in the identification strategy.

Ultimately, continued work on NNs and their application to this problem could result in dedicated hardware that might have the capability to determine not only events of positive acceleration gradient, but also provide dynamic monitoring of the variable status of independent parameters of the experiment and so adapt to the changing environment of the experiment.

Certainly, just using the conventional computer controlled data acquisition system, one would alter the experiment by starting each run with a set of L0 images that would provide information for online cuts during acquisition and/or whether additional beam tuning was required before starting a run or during the course of a run as well as when to terminate a run.

Acknowledgments

I would like to thank the United States Department of Energy – Office of Science for giving me the opportunity to participate in the ERULF program.

I would also like to thank my mentor Dr. James E. Spencer for his maturity and wisdom in guiding me through this research, Advanced Accelerator Research Group B and the entire staff of the Stanford Linear Accelerator Center as well as Sekazi Mtingwa and program director Helen Quinn .

References

[i] T. Plettner et al, (1999) "The laser driven accelerator experiment at Stanford University", Particle Accelerator Conference. New York, N. Y.

[ii] T. Plettner et al, (2001) "Progress of the laser driven accelerator experiment at Stanford University", Particle Accelerator Conference. Chicago, Il l

[iii] T. Plettner et al. Op cit

[iv] Spencer, J. E. (May16-19, 1989) *Real-Time Applications of Neural Nets.* Williamsburg, Va: Real Time Computer Applications in Nuclear Particle and Plasma Physics.